Optical Materials 95 (2019) 109239

Contents lists available at ScienceDirect

Optical Materials

journal homepage: www.elsevier.com/locate/optmat

Ultrafast excited state dynamics and femtosecond nonlinear optical properties of laser fabricated Au and $Ag_{50}Au_{50}$ nanoparticles

K.N. Krishnakanth[a], Byram Chandu[a], M.S.S. Bharathi[a], Sai Santhosh Kumar Raavi[b], S. Venugopal Rao[a,*]

[a] Advanced Research Centre for High Energy Materials (ACRHEM), University of Hyderabad, Hyderabad, 500046, Telangana, India
[b] Ultrafast Photophysics and Photonics Laboratory, Department of Physics, Indian Institute of Technology Hyderabad, Kandi, 502285, Telangana, India

ARTICLE INFO

Keywords:
Femtosecond
Transient absorption
Ablation
Electron thermalization

ABSTRACT

The localized surface plasmon dynamics of laser ablated gold and gold-silver alloy nanoparticles (NPs) near interband and intraband excitation wavelengths were investigated using femtosecond (fs) transient absorption spectroscopy. Interband excitation with 70 fs laser pulses at a wavelength of 400 nm demonstrated plasmon photo-bleach and a transient absorption in the wings of the bleach spectrum. With intraband excitation, $Ag_{50}Au_{50}$ alloy NPs depicted a fast electron thermalization time of ~180 fs. A slower decay of positive absorption from alloy NPs was observed when compared to pure Au NPs. These NPs demonstrated a rapid initial electron thermalization and exhibited similar electron-phonon relaxation times. The third-order nonlinear optical (NLO) properties were measured using the Z-scan technique with 1 kHz repetition rate fs pulses at 800 nm. It is observed that the alloy NPs possessed large value of the NLO susceptibility $\chi^{(3)}$ ($\sim 10^{-13}$ esu) compared to pure gold NPs at 800 nm finding applications in different areas of photonics.

1. Introduction

Metal and metal alloy nanoparticles (NPs) or colloids have fascinating physical and electrical properties depending on their shape and size, which has a tremendous potential in catalytic reactions and plasmonic lasers [1–3]. The nonlinear optical (NLO) properties of gold (Au) and gold-silver (Au–Ag) alloy NPs have attracted significant interest in numerous fields for various applications [4,5]. The Au NPs exhibit the surface plasmon modes in the visible region due to the oscillations of conduction electrons. The plasmon peak mainly depends on the size and shape of the NPs, as the size increases the peak shifts to the red and broadens [6,7]. The major benefit of doping metal NPs with semiconductors is the tunability of intrinsic plasmon band over the visible-NIR spectral region. Additionally, the metal NPs are good light absorbers enabling them create highly excited electron-hole pairs and these charge carriers boost the photo-catalysis and solar energy conversion applications [8,9]. Recently, ultrafast electron relaxation processes involving localized surface plasmons has been demonstrated to be the basis for the high performance of optical switching devices based on the metal nanostructures [10–13]. The electron dynamics and the third order NLO properties of metal and metal-alloy NPs by different spectroscopic techniques are well studied [14–20], in search of unique optoelectronic and switching device applications [11–13,20]. Over the last decade, many research groups have investigated the electron dynamics of Au and Ag–Au alloy NPs synthesized using different approaches either in solution form or in thin film using the techniques of pump-probe or femtosecond (fs) transient absorption spectroscopy [13,21–29].

The geometry of the NPs significantly affect the NLO properties and the corresponding ultrafast electron dynamics in the excited states [30,31]. The heat capacity of the electron is smaller than the heat capacity of the lattice and, therefore, we can selectively excite and monitor the electron dynamics in real time. Following the laser pulse excitation, the electrons relax through internal thermalization by electron-electron collision followed by electron-phonon coupling from external thermalization [23–25]. The non-thermal (non-Fermi) electron distribution following intense laser excitation above the Fermi level has been probed by various techniques [9,27,28]. Electron thermalization dynamics at intraband and interband excitation in mixed metal NPs are not explored much. Recently, Zhang et al. [10] studied the interband and intraband contribution to localized surface plasmon oscillations in pure Au NPs, wherein they have observed a red-shifted induced localized surface plasmon resonance (LSPR) feature with 400 nm pumping. When pumped above the threshold energy of 2.38 eV, it induces the

* Corresponding author.
E-mail addresses: soma_venu@uohyd.ac.in, svrsp@uohyd.ernet.in (S.V. Rao).

https://doi.org/10.1016/j.optmat.2019.109239
Received 2 April 2019; Received in revised form 27 June 2019; Accepted 4 July 2019

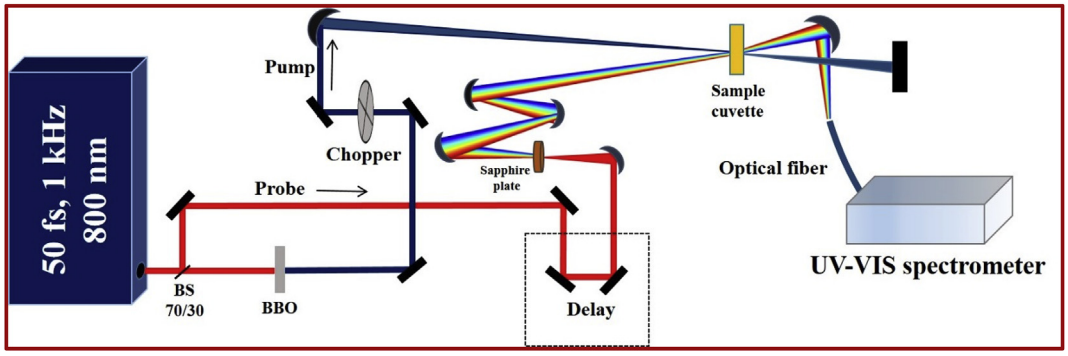

Fig. 1. Experimental schematic of the fs-transient absorption spectrometer.

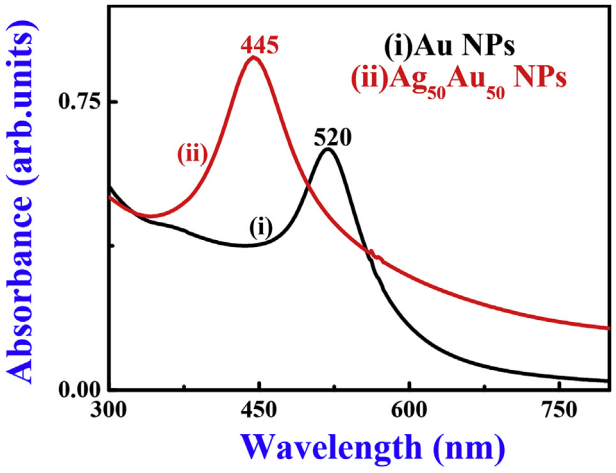

Fig. 2. UV–Visible spectra of as-fabricated NPs (i) Au (ii) $Ag_{50}Au_{50}$ obtained in DW using fs laser ablation with a pulse energy of 500 μJ.

electronic transition from 5d band to the 6sp band resulting in transient increase of population in the conduction band. The excited 5d electrons relax with a typical time delay of 1 ps and this has been demonstrated recently [10]. In this work we have investigated the ultrafast electron thermalization dynamics of Au and $Ag_{50}Au_{50}$ NPs using fs transient absorption spectroscopy. These NPs were achieved through simple and fast approach of ultrafast laser ablation in liquid (ULAL). We observed a fast internal thermalization of non-Fermi electron distribution in Au and $Ag_{50}Au_{50}$ NPs. The measured decay times confirmed the faster response from $Ag_{50}Au_{50}$ alloy nanoparticles compared to pure Au NPs. Furthermore, the third order nonlinear optical (NLO) properties were also measured using the Z-scan technique at 800 nm wavelength with femtosecond, 1 kHz pulses.

2. Experimental details

Gold (Au) and silver-gold ($Ag_{50}Au_{50}$, bulk target) nanoparticles (NPs) were fabricated by the technique of femtosecond (fs) laser ablation of the bulk target (Au/$Ag_{50}Au_{50}$) immersed in the liquid (distilled water). Briefly, bulk targets Au and $Ag_{50}Au_{50}$ (purity 99%, thickens 1 mm) were immersed in distilled water (DW) and irradiated by ultrashort laser pulses from a fs amplifier (LIBRA, Coherent) operating at 800 nm and a repetition rate of 1 kHz with a pulse duration of ~50 fs. The laser pulses were focused on to the target material using the Plano-convex lens (f = 100 mm), which is placed in 5 ml of DW and the covered liquid layer height above the target surface was about 6 mm.

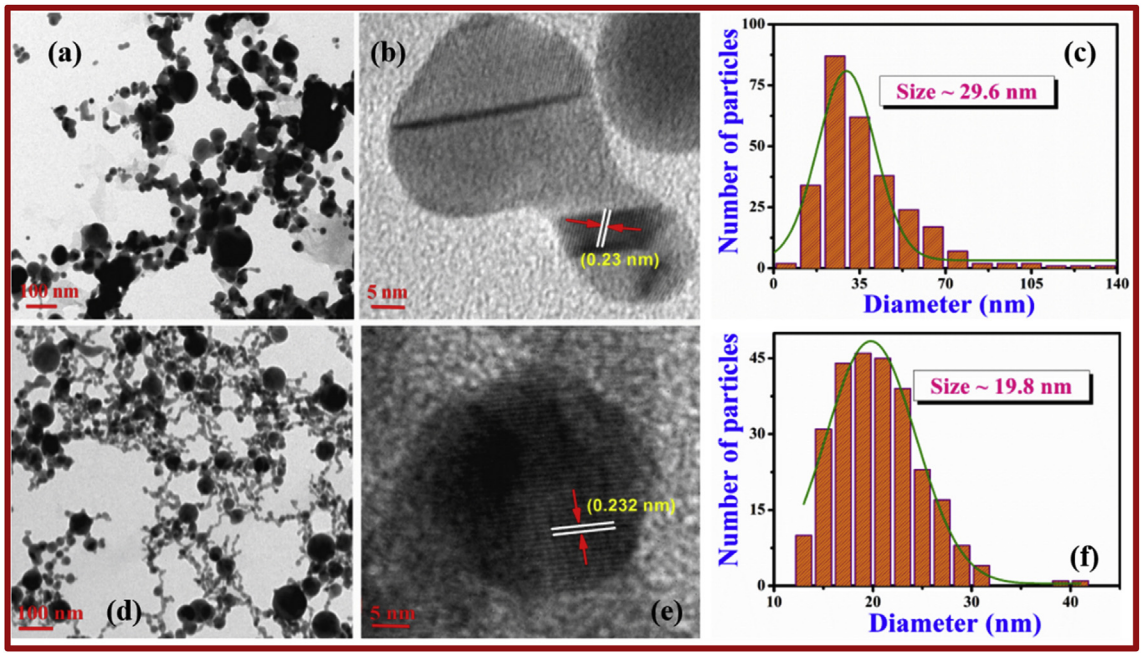

Fig. 3. TEM, HRTEM and size distribution images of as-fabricated NPs (a, b, and c) Au, (d, e and f) $Ag_{50}Au_{50}$, respectively. Inset of (b) and (e) shows their corresponding lattice parameters of Au and $Ag_{50}Au_{50}$ NPs, respectively.

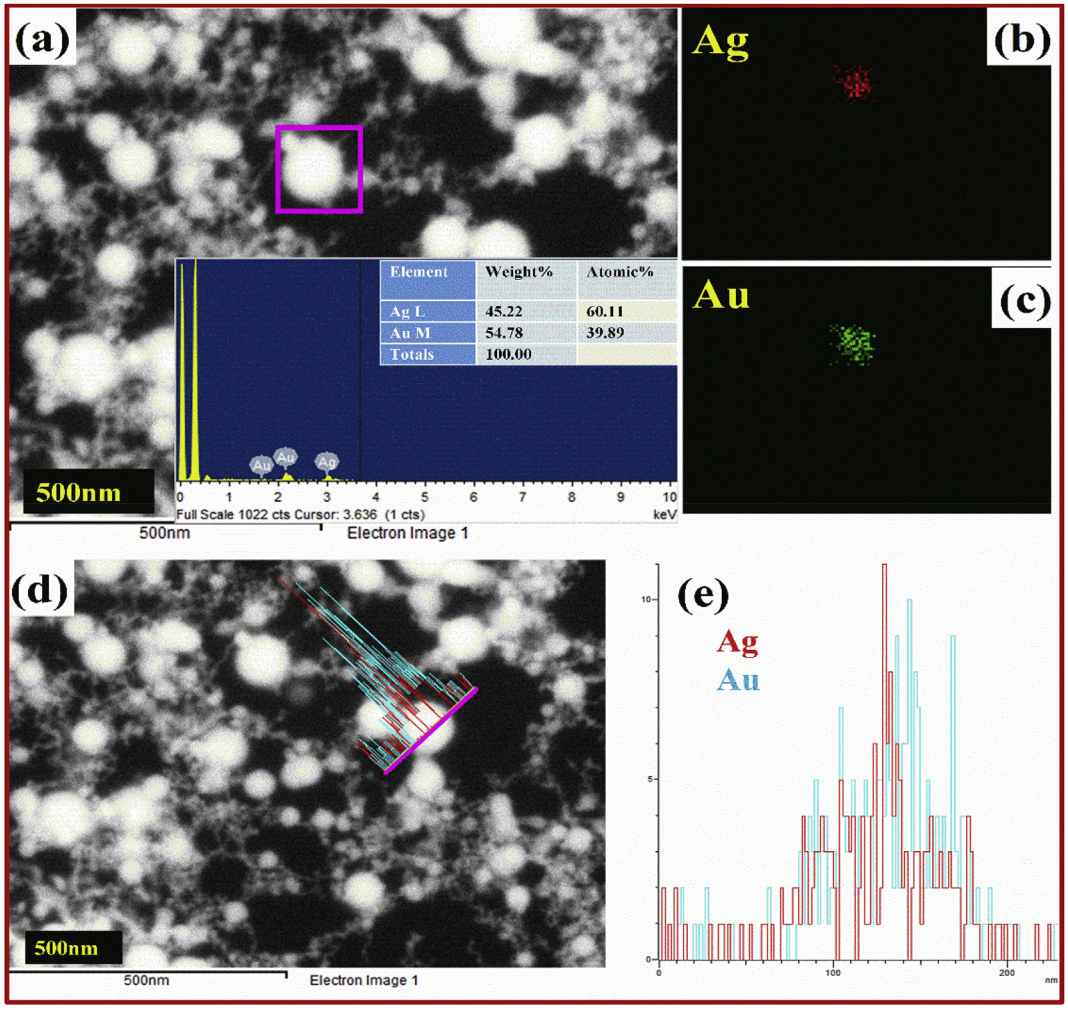

Fig. 4. (a) FESEM image of $Ag_{50}Au_{50}$ NPs with a single map of NP (pink color box) and inset demonstrating the EDS spectra (b) EDS map of Ag. (c) EDS map of Au. (d) Line profile of the $Ag_{50}Au_{50}$ particle indicating the presence of Ag and Au (e) Intensity distribution of both atoms (Ag and Au). (For interpretation of the references to color in this figure legend, the reader is referred to the Web version of this article.)

During the ablation, the target was translated using a computer-controlled X–Y motorized stage with stage velocities of 0.1 mm/s along both directions (X and Y). The experiments were executed at the pulse energy of 500 μJ, and the calculated spot size on the target surface is 100 μm. After the fabrication, NPs were collected in air tightened glass bottles and stored at room temperature. The NPs absorption studies were performed using a UV–Visible (PerkinElmer Lambda 750) spectrometer in the 250–1000 nm wavelength range. The morphological studies of NPs were investigated by high-resolution transmission electron microscope (HRTEM, FEI Tecnai G^2 S-Twin) and selected area diffraction patterns (SAED). The NP compositions and line map images were obtained by field emission scanning electron microscope (FESEM, Carl Zeiss) and energy dispersive X-ray spectroscopy (EDX) techniques.

Femtosecond transient absorption measurements were performed using a transient absorption spectrometer (HELIOS) based on a fs laser system (shown in Fig. 1). A part of the laser output (~4 mJ) from the amplifier (LIBRA, M/s Coherent) was focused on to a 2-mm thick sapphire plate to generate white light probe in the wavelength range of 420–800 nm. A set of parabolic mirrors were used to minimize the chirp of the probe beam. An optical parametric amplifier (OPA) used to tune the wavelength of the laser system and to selectively choose the pump beam. The obtained NPs were pumped at 800 nm and 400 nm wavelength and probed by white continuum (WLC). Both the pump and probe beams were focused on to quartz cuvette (1 mm) with the pump beam chopped at a frequency of 500 Hz to increase the signal-to-noise ratio. The probe beam passed through a delay line to control the delay between the pump and probe pulses with a resolution of (10 fs). The energies of the pump laser used were in the range of 1–2 μJ. The transmitted probe beam was focused on to optical fiber connected with a spectrometer and CCD. The contributions from water and cuvette in these measurements were minimal.

3. Results and discussions

Fig. 2 illustrates the UV–Visible absorption spectra of as-fabricated NPs in DW using fs ablation. As evident from the data illustrated in Fig. 2, a single plasmon peak was observed at 445 nm for $Ag_{50}Au_{50}$ NPs clearly indicating that there was no core-shell formation in the obtained colloidal solution. We expect two plasmon bands if there were any core-shell NPs in contrast to the Ag–Au bimetallic NPs. From Fig. 2, it is evident that the observed absorption maxima at 520 nm demonstrates the formation of spherical Au NPs. Moreover, the observed plasmon band for bimetallic NPs was located in region between that of the pure Ag and Au NPs, which is in good agreement with the observations from earlier reports. Moreover, absorption band intensity was higher for $Ag_{50}Au_{50}$ NPs than the Au NPs, which could be ascribed to the variation in ablation thresholds of the individual metals. In one of our earlier reports, we demonstrated the smooth tuning of bimetallic NPs plasmon bond while changing the Au proportion in laser ablation experiments [32,33].

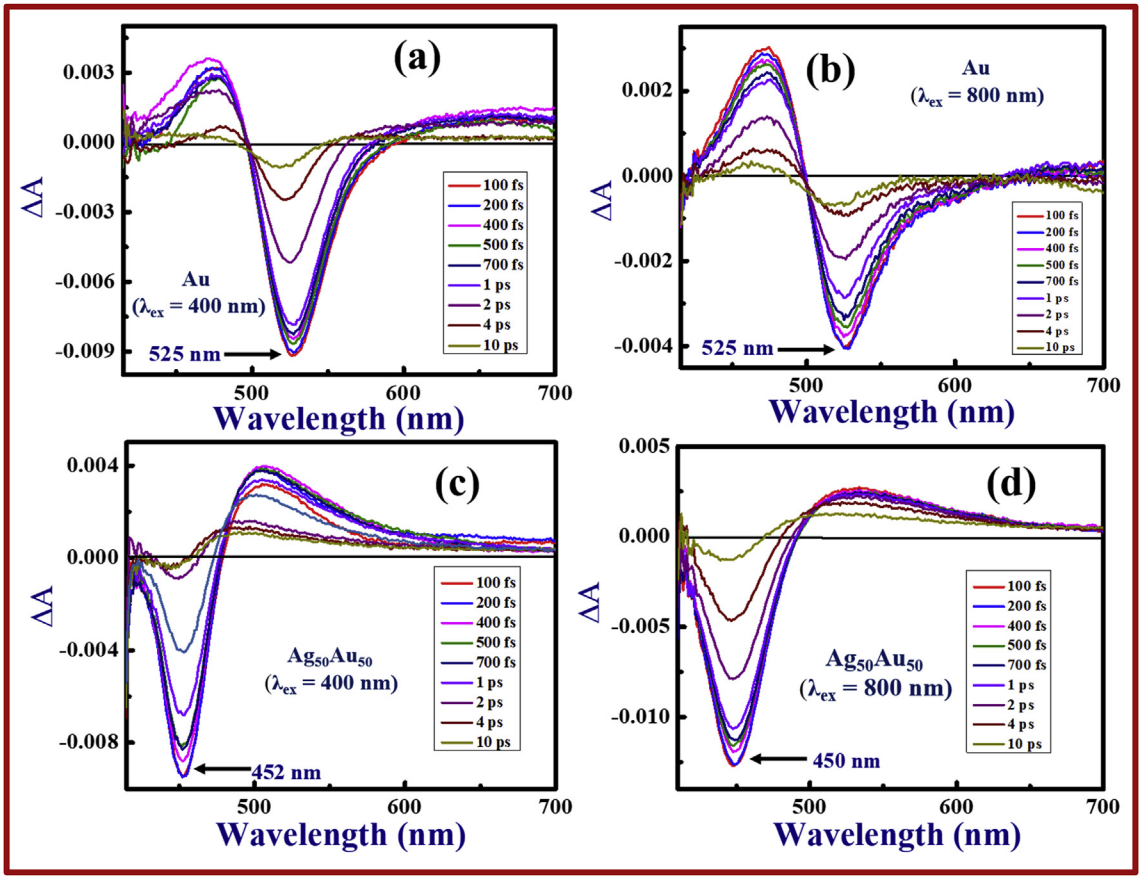

Fig. 5. Transient absorption spectra of (a, b) Au and (c, d) Au–Ag NPs in DW pumped at 400 nm and 800 nm wavelength and the insets show their corresponding kinetic spectra of surface plasmon.

Table 1
Individual decay constants of Au and $Ag_{50}Au_{50}$ with intraband (800 nm) and interband (400 nm) excitation.

Time constants	Au (λ_{ex} = 400 nm)	Au (λ_{ex} = 800 nm)	$Ag_{50}Au_{50}$ (λ_{ex} = 400 nm)	$Ag_{50}Au_{50}$ (λ_{ex} = 800 nm)
τ1	0.31 ± 0.03 ps	0.4 ± 0.04ps	0.25 ± 0.01 ps	0.15 ± 0.01 ps
τ2	1.26 ± 0.02 ps	1.2 ± 0.08 ps	1.67 ± 0.03 ps	3.26 ± 0.04 ps
τ3	35 ± 0.02 ps	34 ± 0.03 ps	35 ± 0.06 ps	22 ± 0.08 ps

Morphological studies and crystallographic phases of as-fabricated NPs were obtained from the analysis of the TEM and HRTEM data, respectively. Fig. 3(a) and (b) depict the TEM and HRTEM micrographs of the Au NPs. Most of NPs had a spherical shape with interconnected structures and their diameters were estimated to be in the range of 10–140 nm. Inset of Fig. 3(b) demonstrates the interplanar spacing of Au NPs (0.23 nm) corresponding to the (111) Miller plane. Fig. 3(d) and (e) illustrate the TEM and HRTEM images of $Ag_{50}Au_{50}$ NPs and the diameters were found to be in the range of 15–50 nm. Inset of Fig. 3(e) illustrates the lattice plane separation of 0.232 nm for $Ag_{50}Au_{50}$ NPs, which is assigned to the Miller plane of (111). Moreover, the $Ag_{50}Au_{50}$ interplanar separation is comparable to the pure Ag and Au phases because of the similar lattice constants [a = 4.09 Å (Ag), a = 4.08 Å (Au)] of Ag and Au. The NPs mean size was estimated by counting > 250 particles using the image-J software and the obtained mean sizes were ~29.6 nm and ~19.8 nm for Au NPs [Fig. 3(c)] and $Ag_{50}Au_{50}$ NPs [Fig. 3(f)], respectively.

Further, FESEM-EDX mapping was performed on $Ag_{50}Au_{50}$ single particle to identify the distribution and composition of both atoms. Fig. 4(a) illustrates the EDS map on the single particle ($Ag_{50}Au_{50}$ NP) represented with rectangular box (pink color) and parts (b) and (c) of Fig. 3 confirmed the presence of both atoms [Ag (the red one), Au (the yellow one)]. EDX spectra presented in the inset of Fig. 4(a) demonstrates the individual Ag and Au atoms composition with weight percentages of 45.2% and 54.7%, respectively. Fig. 4(d)–(e) depict the data from a line scan on single NP, clearly signifying the particle comprised of both Ag and Au atoms. Briefly, the bimetallic NPs formation during laser ablation of the target can be explained as follows. When a focused fs pulse interacts with the target (in liquid) extremely high temperature and pressure are induced at the target-liquid interface. During the laser irradiation, atoms/ions can be ejected via the vaporization followed by the generation of dense metal atoms (Ag and Au) near the focal spot. The ejected metal atoms will aggregate and generate bimetallic NPs owing to the strong interaction between the individual metal atoms than the solvent and metal. Therefore, the formed bimetallic NPs will be homogeneous because of their thermodynamically favorable mixing process at any proportion [34].

Fig. 5 shows the transient absorption spectra (TAS) of (a, b) Au and (c, d) $Ag_{50}Au_{50}$ NPs at different probe delay times. Following the laser excitation photo-bleach of the plasmonic band and a transient absorption spectrum at the wings of the bleached spectrum was observed. As time delay between the pump and probe pulses increased the transient absorption spectra decayed and the bleached spectrum recovered. With 400 nm excitation, pure Au NPs illustrated a negative band centered at

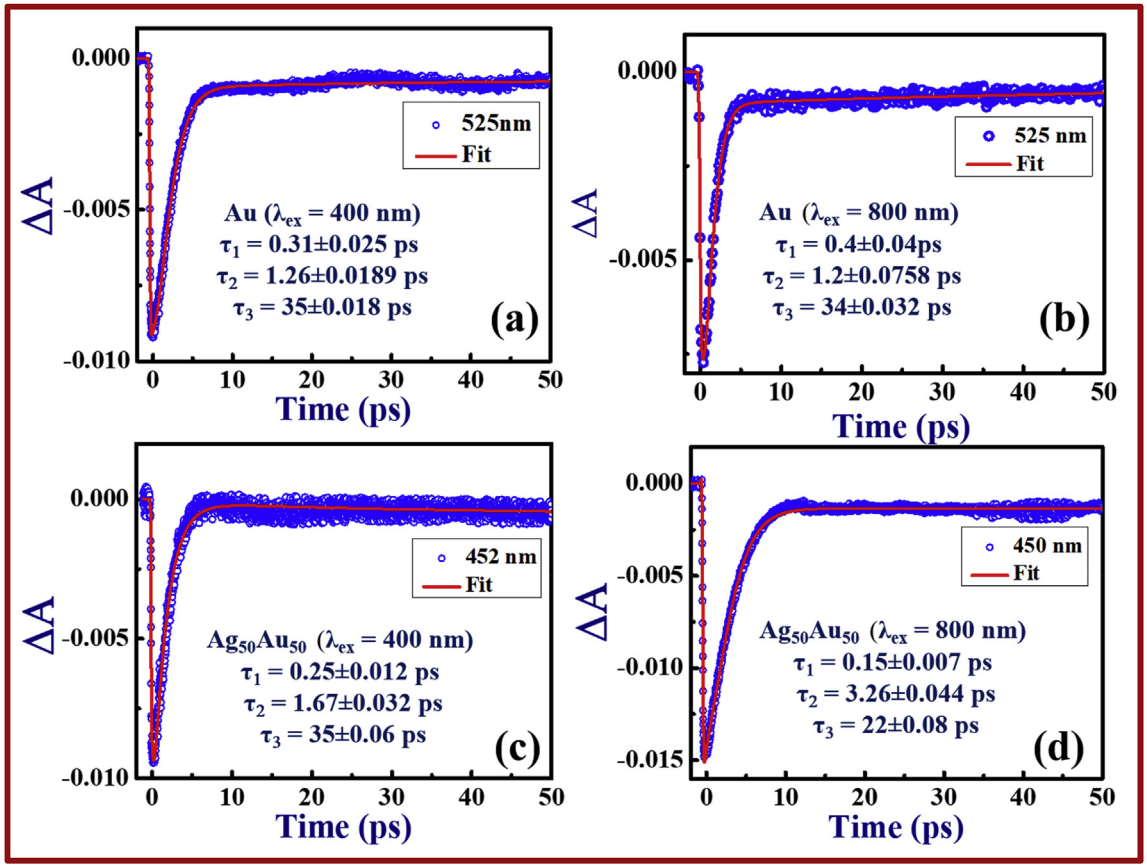

Fig. 6. The intrinsic Plasmon bleach recovery of (a, b) Au and (c, d) $Ag_{50}Au_{50}$ NPs. Open circles are the experimental data points while the solid curves are theoretical fits.

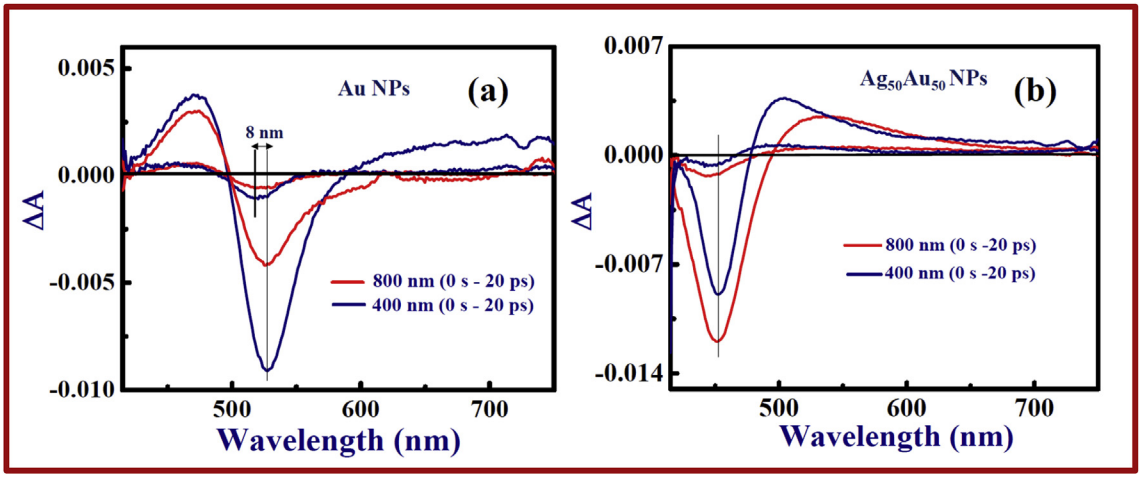

Fig. 7. Transient absorption spectra of (a) Au and (b) $Ag_{50}Au_{50}$ NPs at delay increasing from 0 to 20 ps for 400 nm and 800 nm pump wavelength.

525 nm, which could be due to the depletion of the plasmon electrons. Another positive band placed above 600 nm could be attributed to absorption of thermally excited non-equilibrium electron distribution near Fermi level. Near the intraband excitation (800 nm wavelength) the positive absorption band above 600 nm disappeared [as seen in Fig. 4(b) data] clearly suggesting the oscillation of conduction band electrons. In the case of $Ag_{50}Au_{50}$ NPs, an intense photo-bleach spectrum is observed at ~450 nm and a photo-induced absorption above 500 nm wavelength with both intraband and interband excitations.

The representative kinetics of the photo-bleached plasmonic bands was fitted using a triple exponential function ($y = y_0 + A_1 \times \exp[-(x-x_0)/t_1] + A_2 \times \exp[-(x-x_0)/t_2] + A_3 \times \exp[-(x-x_0)/t_3]$) Three lifetimes were required to adequately fit (using a MATLAB program and Surface Xplorer) the transient kinetics of Au and $Ag_{50}Au_{50}$ NPs and the data obtained from the fits obtained is summarized in Table 1. With both interband and intraband excitation $Ag_{50}Au_{50}$ NPs exhibited a faster response compared to pure Au NPs and is evident from the data presented in Fig. 6. The obtained three lifetimes are ascribed to the internal electron-electron, electron-phonon and phonon-phonon scattering mechanisms, respectively [14–17].

The interband excitation of pure Au NPs depicted a blue-shifted plasmon resonance peak compared to intraband excitation energies as

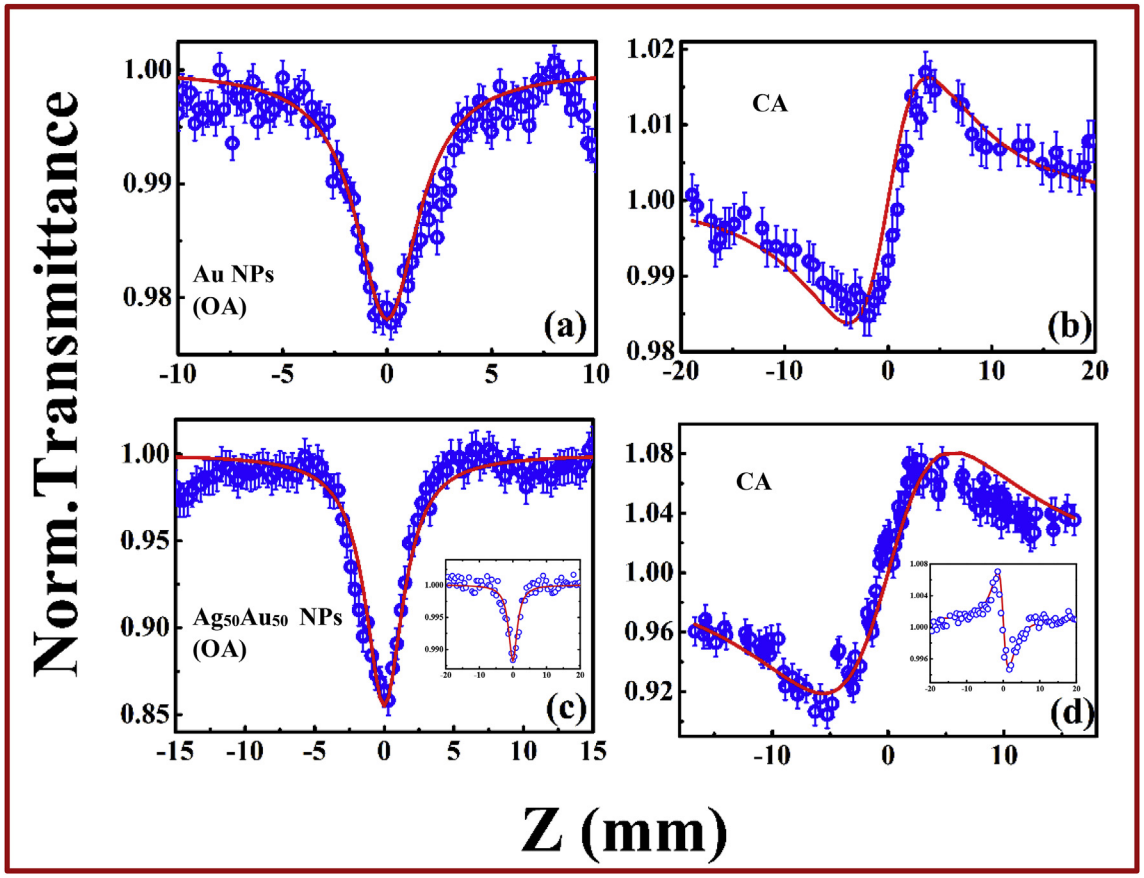

Fig. 8. Open (a) and (c), closed (b) and (d) aperture Z-scan curves for laser ablated (a, b) Au and (c, d) $Ag_{50}Au_{50}$ NPs, respectively. Insets of (c) and (d) illustrate the solvent (water) NLO response. Open circles are the experimental data points while the solid curves are theoretical fits.

Table 2
NLO coefficients of the Au and $Ag_{50}Au_{50}$ alloy NPs obtained at 800 nm wavelength using fs Z-scan data.

NPs	β (m/W)	$\sigma^{(2)}$ GM	n_2 (m^2/W)	$\chi^{(R)}$(m^2/V^2)	$\chi^{(I)}$(m^2/V^2)	$\chi^{(3)}$(m^2/V^2)	$\chi^{(3)}$ (esu)
Au NPs	0.4×10^{-12}	1.1×10^{5}	3.2×10^{-20}	3.0×10^{-22}	2.7×10^{-22}	4.0×10^{-22}	2.8×10^{-14}
$Ag_{50}Au_{50}$ NPs	5.0×10^{-12}	4.0×10^{5}	1.6×10^{-19}	1.5×10^{-21}	3.0×10^{-21}	3.3×10^{-21}	2.4×10^{-13}
Water	8.1×10^{-14}	–	2.2×10^{-21}	2.1×10^{-23}	4.9×10^{-25}	2.1×10^{-23}	1.5×10^{-15}

shown in Fig. 7. It is clear that the positive absorption above 600 nm, called the interband excitation induced plasmon (EIP) [10], decays slowly (~3.5 ps) when compared to the intrinsic plasmon peak. When the time delay reached 20 ps the intrinsic plasmon (IP) peak was blue shifted by 8 nm at 400 nm pumping due to the influence of EIP on IP. The TA spectra [Fig. 7(b)] of $Ag_{50}Au_{50}$ alloy NPs at 400 nm and 800 nm excitations show a intrinsic plasmon photo-bleach peak near 450 nm and a positive absorption EIP like process above 490 nm. The photo-bleach (PB) spectral band was observed to be broader upon photo-excitation with 800 nm when compared to that of the data obtained with 400 nm. The positive peak decayed faster at interband excitation with lifetimes of 1.94 ps and 7.6 ps. The electron dynamic process of the bleached plasmonic band shows faster electron–electron scattering compared to pure Au NPs (Fig. 6). From Fig. 7(b) data we observe that as we increased the delay, the bleached plasmonic band recovered with decreasing positive absorption with no change in the resonant bleached spectrum.

The synthesized Au and $Ag_{50}Au_{50}$ NPs third-order NLO properties have also been investigated using the Z-scan technique with 800 nm fs pulses. The complete experimental details can be found in our previous work [35]. Fig. 8 shows the open and closed aperture Z-scan data of Au and $Ag_{50}Au_{50}$ NPs measured at a peak intensity of 40 GW/cm^2. Fig. 8(a) and (c) illustrate the open aperture (OA) Z-scan curves clearly depicting a reverse saturable absorption (RSA) behavior for all the NPs. The obtained data were fitted using a two-photon absorption (2 PA) equation [35] and the estimated value of β was 0.4×10^{-12}, and 5.0×10^{-12} m/W for Au and $Ag_{50}Au_{50}$ NPs, respectively. From the obtained 2 PA values $Ag_{50}Au_{50}$ alloy NPs clearly shows stronger NLO coefficients compared to pure Au NPs.

Figures 8(b) and (d) illustrate the closed aperture (CA) curves for laser ablated Au and $Ag_{50}Au_{50}$ NPs, respectively. The data evidently exhibited self-focusing effect and the curves were fitted using the standard equations for closed aperture Z-scan [35]. The valley followed by a peak in the normalized transmittance data clearly suggests that the sample possessed a positive type of nonlinearity and obtained values of n_2 are 3.2×10^{-20} m^2/W and 1.6×10^{-19} m^2/W for Au and Ag–Au alloy NPs, respectively. Two-photon absorption cross-sections $\sigma^{(2)}$ are calculated using the relation β × E/N, where E is the energy of photon, N is the number density (per cc) [35]. Because of errors in the fluctuations of laser power, estimation of beam waist and fitting procedures, ± 10% errors are expected in the coefficients reported here. Ganeev et al. investigated the nonlinear optical properties of Ag NPs [36] prepared by

laser ablation in various liquids and calculated nonlinear absorption coefficient as 3×10^{-9} cm/W at 397.5 nm, and 8×10^{-9} cm/W at 795 nm. Further, they have also studied the NLO coefficients of Au NPs and the values were -8×10^{-14} m^2/W and 1.7×10^{-10} m/W [37]. The obtained NLO coefficients from the present study are summarized in Table 2. The NLO coefficients of the metal colloids mainly depends on the metal (size and shape), matrix and the Plasmon resonance. Also, the dimensional reduction of the conduction electrons and the interband and intraband transitions (which leads to a bleaching of the Plasmon band), certainly determines the absorption properties [38–41]. Recently, Palpant et al. demonstrated the influence of pulse duration on the absorption cross section of the gold nanorods which shows the increase in absorption cross section with sub picosecond pulses [42]. Here, the obtained NLO parameters have contributions both from the metal NPs and the solvent (water) and the obtained NLO coefficients are relatively similar to the differently synthesized metal NPs [11,43–45]. Apart from the oxide layer formation on laser ablated NPs in liquid, the mechanism of LAL is robust and chemical free, which can be used for optical limiting, saturable absorbers and biological applications.

4. Conclusions

In conclusion, we have successfully synthesized the Au and $Ag_{50}Au_{50}$ composite NPs using LAL process with an average diameter in between 15 and 30 nm. The electron-electron relaxation times were obtained for $Ag_{50}Au_{50}$ alloy NPs and have a fast response at both inter and intraband excitation. Both the NPs have similar electron-phonon relaxation times, which shows homogeneity of the composite material. The obtained electron dynamics from these NPs are exhibiting fast response compared to other studies on Au and $Ag_{50}Au_{50}$ nanocomposite materials [29,30]. The third-order nonlinear optical susceptibility of alloy NPs have stronger values compared to pure Au NPs measured at 800 nm wavelength. The tunability of the plasmonic band and the fast response of these nanocomposite materials are prerequisite in optical switching devices and biological applications.

Declaration of interests

The authors declare that they have no known competing financial interests or personal relationships that could have appeared to influence the work reported in this paper.

The authors declare the following financial interests/personal relationships which may be considered as potential competing interests:

Acknowledgments

We thank DRDO, India for financial support through the project sanction #ERIP/ER/1501138/M/01/319/D (R&D) dated 27.02.2017. RSSK acknowledges the financial support for the following projects nos. DST/YSS/2015/000008, BRICS/PilotCall2/IEEE-OSC/2018 (G) and SPARC/2018–2019/P301/SL.

References

[1] Y. Li, J.Y. Lan, J. Liu, J. Yu, Z. Luo, W. Wang, L. Sun, Synthesis of gold nanoparticles on rice husk silica for catalysis applications, Ind. Eng. Chem. Res. 54 (2015) 5656–5663, https://doi.org/10.1021/acs.iecr.5b00216.
[2] K.-M. Sung, D.W. Mosley, B.R. Peelle, S. Zhang, J.M. Jacobson, Synthesis of monofunctionalized gold nanoparticles by Fmoc solid-phase reactions, J. Am. Chem. Soc. 126 (2004) 5064–5065.
[3] P. Suchomel, L. Kvitek, R. Prucek, A. Panacek, A. Halder, S. Vajda, R. Zboril, Simple size-controlled synthesis of Au nanoparticles and their size-dependent catalytic activity, Sci. Rep. 8 (2018) 4589.
[4] E.J. Heilweil, R.M. Hochstrasser, Nonlinear spectroscopy and picosecond transient grating study of colloidal gold, J. Chem. Phys. 82 (1985) 4762–4770.
[5] M.J. Bloemer, J.W. Haus, P.R. Ashley, Degenerate four-wave mixing in colloidal gold as a function of particle size, J. Opt. Soc. Am. B 7 (1990) 790–795.
[6] M. Kerker, The Scattering of Light and Other Electromagnetic Radiation: Physical Chemistry: A Series of Monographs, Academic Press, 2013.
[7] C.F. Bohren, D.R. Huffman, Absorption and Scattering of Light by Small Particles, John Wiley & Sons, 2008.
[8] A. Rana, N. Gupta, A. Lochan, G.D. Sharma, S. Chand, M. Kumar, R.K. Singh, Charge carrier dynamics and surface plasmon interaction in gold nanorod-blended organic solar cell, J. Appl. Phys. 120 (2016) 63102.
[9] G. V Hartland, L. V Besteiro, P. Johns, A.O. Govorov, What's so hot about electrons in metal nanoparticles? ACS Energy Lett. 2 (2017) 1641–1653.
[10] X. Zhang, C. Huang, M. Wang, P. Huang, X. He, Z. Wei, Transient localized surface plasmon induced by femtosecond interband excitation in gold nanoparticles, Sci. Rep. 8 (2018) 10499.
[11] Y. Zhang, Y. Wang, Nonlinear optical properties of metal nanoparticles: a review, RSC Adv. 7 (2017) 45129–45144.
[12] M. Ren, B. Jia, J. Ou, E. Plum, J. Zhang, K.F. MacDonald, A.E. Nikolaenko, J. Xu, M. Gu, N.I. Zheludev, Nanostructured plasmonic medium for terahertz bandwidth all-optical switching, Adv. Mater. 23 (2011) 5540–5544.
[13] Y. Lin, X. Zhang, Ultrafast multipolar plasmon for unidirectional optical switching in a hemisphere-nanoshell array, Adv. Opt. Mater. 5 (2017) 1601088.
[14] S. Link, C. Burda, Z.L. Wang, M.A. El-Sayed, Electron dynamics in gold and gold–silver alloy nanoparticles: the influence of a nonequilibrium electron distribution and the size dependence of the electron–phonon relaxation, J. Chem. Phys. 111 (1999) 1255–1264.
[15] T.S. Ahmadi, S.L. Logunov, M.A. El-Sayed, Picosecond dynamics of colloidal gold nanoparticles, J. Phys. Chem. 100 (1996) 8053–8056.
[16] H.F. Zarick, A. Boulesbaa, E.M. Talbert, A. Puretzky, D. Geohegan, R. Bardhan, Ultrafast excited-state dynamics in shape-and composition-controlled gold–silver bimetallic nanostructures, J. Phys. Chem. C 121 (2017) 4540–4547.
[17] L.C. Du, W.D. Xi, J.B. Zhang, H. Matsuzaki, A. Furube, Electron transfer dynamics and yield from gold nanoparticle to different semiconductors induced by plasmon band excitation, Chem. Phys. Lett. 701 (2018) 126–130.
[18] T. Zhao, P.J. Herbert, H. Zheng, K.L. Knappenberger Jr., State-resolved metal nanoparticle dynamics viewed through the combined lenses of ultrafast and magneto-optical spectroscopies, Acc. Chem. Res. 51 (2018) 1433–1442.
[19] N. Del Fatti, F. Vallee, Ultrafast optical nonlinear properties of metal nanoparticles, Appl. Phys. B 73 (2001) 383–390.
[20] Y. Takeda, O.A. Plaksin, J. Lu, N. Kishimoto, Optical switching performance of metal nanoparticles fabricated by negative ion implantation, Nucl. Instrum. Methods Phys. Res. Sect. B Beam Interact. Mater. Atoms 242 (2006) 194–197.
[21] C. Voisin, N. Del Fatti, D. Christofilos, F. Vallée, Ultrafast Electron Dynamics and Optical Nonlinearities in Metal Nanoparticles, (2001).
[22] R.D. Averitt, S.L. Westcott, N.J. Halas, Ultrafast electron dynamics in gold nanoshells, Phys. Rev. B 58 (1998) R10203.
[23] H.E. Elsayed-Ali, T. Juhasz, G.O. Smith, W.E. Bron, Femtosecond thermoreflectivity and thermotransmissivity of polycrystalline and single-crystalline gold films, Phys. Rev. B 43 (1991) 4488.
[24] O.B. Wright, Ultrafast nonequilibrium stress generation in gold and silver, Phys. Rev. B 49 (1994) 9985.
[25] R.W. Schoenlein, W.Z. Lin, J.G. Fujimoto, G.L. Eesley, Femtosecond studies of nonequilibrium electronic processes in metals, Phys. Rev. Lett. 58 (1987) 1680.
[26] C.-K. Sun, F. Vallée, L.H. Acioli, E.P. Ippen, J.G. Fujimoto, Femtosecond-tunable measurement of electron thermalization in gold, Phys. Rev. B 50 (1994) 15337.
[27] W.S. Fann, R. Storz, H.W.K. Tom, J. Bokor, Direct measurement of nonequilibrium electron-energy distributions in subpicosecond laser-heated gold films, Phys. Rev. Lett. 68 (1992) 2834.
[28] J.G. Fujimoto, J.M. Liu, E.P. Ippen, N. Bloembergen, Femtosecond laser interaction with metallic tungsten and nonequilibrium electron and lattice temperatures, Phys. Rev. Lett. 53 (1984) 1837.
[29] P. Johns, G. Beane, K. Yu, G.V. Hartland, Dynamics of surface plasmon polaritons in metal nanowires, J. Phys. Chem. C 121 (2017) 5445–5459.
[30] Y. Hua, K. Chandra, D.H.M. Dam, G.P. Wiederrecht, T.W. Odom, Shape-dependent nonlinear optical properties of anisotropic gold nanoparticles, J. Phys. Chem. Lett. 6 (2015) 4904–4908.
[31] T.E. Karam, H.T. Smith, L.H. Haber, Enhanced photothermal effects and excited-state dynamics of plasmonic size-controlled gold–silver–gold core–shell–shell nanoparticles, J. Phys. Chem. C 119 (2015) 18573–18580.
[32] G.K. Podagatlapalli, S. Hamad, S.V. Rao, Trace-level detection of secondary explosives using hybrid silver–gold nanoparticles and nanostructures achieved with femtosecond laser ablation, J. Phys. Chem. C 119 (2015) 16972–16983.
[33] C. Byram, V.R. Soma, 2, 4-dinitrotoluene detected using portable Raman spectrometer and femtosecond laser fabricated Au–Ag nanoparticles and nanostructures, Nanostruct. Nano-Objects 12 (2017) 121–129.
[34] I. Lee, S.W. Han, K. Kim, Production of Au–Ag alloy nanoparticles by laser ablation of bulk alloys, Chem. Commun. (2001) 1782–1783.
[35] K.N. Krishnakanth, S. Seth, A. Samanta, S. Venugopal Rao, Broadband ultrafast nonlinear optical studies revealing exciting multi-photon absorption coefficients in phase pure zero-dimensional Cs_4PbBr_6 perovskite films, Nanoscale 11 (2019) 945–954.
[36] R.A. Ganeev, M. Baba, A.I. Ryasnyansky, M. Suzuki, H. Kuroda, Characterization of optical and nonlinear optical properties of silver nanoparticles prepared by laser ablation in various liquids, Optic Commun. 240 (2004) 437–448.
[37] R.A. Ganeev, M. Suzuki, M. Baba, M. Ichihara, H. Kuroda, Low-and high-order nonlinear optical properties of Au, Pt, Pd, and Ru nanoparticles, J. Appl. Phys. 103 (2008) 63102.
[38] R. Philip, P. Chantharasupawong, H. Qian, R. Jin, J. Thomas, Evolution of nonlinear optical properties: from gold atomic clusters to plasmonic nanocrystals, Nano Lett. 12 (2012) 4661–4667.

[39] S. Dengler, C. Kübel, A. Sch wenke, G. Ritt, B. Eberle, Near-and off-resonant optical limiting properties of gold–silver alloy nanoparticles for intense nanosecond laser pulses, J. Opt. 14 (2012) 75203.
[40] V.A. Karavanskii, A.V. Simakin, V.I. Krasovskii, P. V Ivanchenko, Nonlinear optical properties of colloidal silver nanoparticles produced by laser ablation in liquids, Quant. Electron. 34 (2004) 644.
[41] H. Pan, W. Chen, Y.P. Feng, W. Ji, J. Lin, Optical limiting properties of metal nanowires, Appl. Phys. Lett. 88 (2006) 223106.
[42] X. Hou, N. Djellali, B. Palpant, Absorption of ultrashort laser pulses by plasmonic nanoparticles: not necessarily what you might think, ACS Photonics 5 (2018) 3856–3863.
[43] J.P. Novak, L.C. Brousseau, F.W. Vance, R.C. Johnson, B.I. Lemon, J.T. Hupp, D.L. Feldheim, Nonlinear optical properties of molecularly bridged gold nanoparticle arrays, J. Am. Chem. Soc. 122 (2000) 12029–12030.
[44] M.H.M. Ara, Z. Dehghani, R. Sahraei, A. Daneshfar, Z. Javadi, F. Divsar, Diffraction patterns and nonlinear optical properties of gold nanoparticles, J. Quant. Spectrosc. Radiat. Transf. 113 (2012) 366–372.
[45] N. Ahmadi, R. Poursalehi, A. Kirilyuk, M.K.M. Farshi, Effect of gold plasmonic shell on nonlinear optical characteristics and structure of iron based nanoparticles, Appl. Surf. Sci. 479 (2019) 114–118.